Micro/nano-fiber-based source of heralded single photons at the telecom band

Jie Su (苏 杰)[1], Liang Cui (崔 亮)[1,*], Yuhang Li (李宇航)[2,3], and Xiaoying Li (李小英)[1]

[1]*College of Precision Instrument and Opto-electronics Engineering, Key Laboratory of Optoelectronics Information Technology of Ministry of Education, Tianjin University, Tianjin 300072, China*

[2]*Joint Institute for Measurement Science, Tsinghua University, Beijing 100084, China*

[3]*Department of Physics, Tsinghua University, Beijing 100084, China*

**Corresponding author: lcui@tju.edu.cn*

Received November 27, 2017; accepted February 1, 2018; posted online March 26, 2018

We experimentally demonstrate a heralded single photon source at 1290 nm by exploiting the spontaneous four wave mixing in a taper-drawn micro/nano-fiber (MNF). Because the frequency detuning between the pump and heralded single photons is ∼58 THz, the contamination by Raman scattering is significantly reduced at room temperature. Since the MNF is naturally connected to standard single mode fibers via fiber tapers, the source would be compatible with the existing fiber networks. When the emission rate of heralded signal photons is about 4.6 kHz, the measured second-order intensity correlation function $g^{(2)}(0)$ is 0.017 ± 0.002, which is suppressed by a factor of more than 55, relative to the classical limit.

OCIS codes: 190.4380, 270.5290.

doi: 10.3788/COL201816.041903.

Single photon sources not only play an important role in fundamental research of quantum mechanics[1,2], but also enable myriad applications in quantum information processing, such as quantum key distribution (QKD) and quantum computing[3–6]. An ideal single photon source would produce completely characterized single photons on demand. However, the best single photon sources that can be achieved are sources that offer some approximations to an ideal one. Heralded single photon sources, which rely on photon pairs produced by spontaneous parametric emissions in $\chi^{(2)}$- or $\chi^{(3)}$-based nonlinear media, are one commonly used approximation. The detection event of one photon from a pair heralds the existence of its correlated counterpart, where the counterpart is thus projected to a single photon state. Since the first experimental demonstration[7], heralded single photons based on spontaneous parametric down conversion in $\chi^{(2)}$-based nonlinear media have been extensively investigated[8–11]. Recently, there are growing interests in realizing heralded single photons by using spontaneous four wave mixing (SFWM) in $\chi^{(3)}$-based optical fibers[12–19], because the fiber-based sources have the potential for being developed into an all-fiber compact source and have higher compatibility with current fiber networks.

So far, heralded single photons have been realized via SFWM in standard single mode fibers (SMFs), dispersion shifted fibers (DSFs), and photonic crystal fibers (PCFs). The SMF- and DSF-based single photon sources[13,14], which rely on the signal and idler photon pairs in telecom O band and C band, respectively, are highly efficient and compatible with standard SMF, but they suffer from the noise that originates from spontaneous Raman scattering (RS). For the PCF-based sources, the contamination by RS can be eliminated by utilizing signal and idler photon pairs with large frequency difference[15,16], and heralded single photons in a pure state can be achieved by properly designing and controlling the dispersion of PCFs[17,18]. However, in practice, splicing a PCF and a standard SMF together with low loss is still a tricky task, since the splicing loss depends on the mode field mismatch of the two fibers and a number of splicing parameters need to be customized for a particular PCF[20].

It has been demonstrated recently that photon pairs can be generated from taper-drawn micro/nano-fibers (MNFs)[21]. Compared with SMF and DSF, a taper-drawn MNF usually has a smaller mode field diameter, which results in a higher nonlinearity, and the dispersion of a MNF can be tailored within a certain extent by controlling the fiber diameter. By tailoring the dispersion of the MNF, the gain spectrum of SFWM can be moved away from the major Raman gain peaks; thus, the contamination of photon pairs by RS can be suppressed. On the other hand, taper-drawn MNFs are naturally connected to SMF via fiber tapers. If the tapers are adiabatic, the transition between MNF and SMF could be lossless. Therefore, compared with PCFs, taper-drawn MNFs offer more convenience for developing an all-fiber source.

In this Letter, we demonstrate a heralded single photon source by utilizing photon pairs generated from a taper-drawn MNF. Generally, our single photon source follows the structure of the photon pair source reported in Ref. [21]. However, characterizations for our source are conducted from a different aspect. The key parameters of a heralded single photon source, such as heralding efficiency and photon statistic properties, are experimentally characterized. Moreover, our source is optimized with a set of wavelengths with lower RS noise. The wavelengths

 © 2018 Chinese Optics Letters

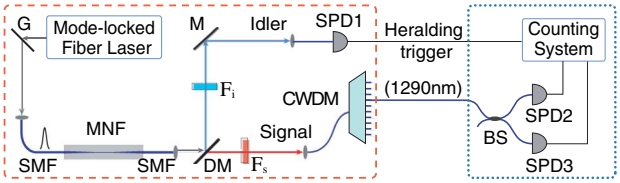

Fig. 1. Experimental setup. The area framed by the dashed line is the heralded single photon source, while the area framed by the dotted line is the measurement system for characterizing the source. G, diffraction grating; SMF, single mode fiber; DM, dichroic mirror; M, mirror; F_s, long-pass filters of signal photons; F_i, bandpass filters of idler photons; CWDM, coarse wavelength division multiplexer; SPD, single photon detector; BS, 50/50 beam splitter.

of the pump and heralded single photons are 1032 and 1290 nm, respectively.

As shown in Fig. 1, our experimental setup consists of two parts, the MNF-based heralded single photon source and the characterization system. The MNF with length and diameter of ~15 cm and ~0.9 μm, respectively, is fabricated by using a taper-drawing workstation. During the taper-drawing process, a SMF with core diameter of ~9 μm is heated by a millimeter-size flame of hydrogen–oxygen mixture and is pulled by using two computer-controlled translation stages in the meantime. To prevent dust contamination and to ease the handling, an as-fabricated MNF and its tapered regions are sealed into a plastic housing. By employing the standard simulation method for air-cladding silica MNFs, we calculate the key parameters of our MNF. According to the calculation, the zero dispersion wavelength of our MNF is ~1115 nm with a nonlinear coefficient of ~63 $W^{-1} \cdot km^{-1}$ at a wavelength of 1 μm. The cutoff wavelength of single mode propagation in our MNF is ~1250 nm, so the single mode condition can be guaranteed for the heralded single photons at 1290 nm.

According to calculated phase matching curve of SFWM in our MNF[21], the frequency detuning between the pump and the emerging signal (idler) photons can be more than 50 THz when the pump wavelength is around 1 μm. This large frequency detuning means the signal and idler photons can avoid the contamination by the major RS peaks from the first-order to the third-order. For our heralded single photon source, we choose an optimized pump wavelength of 1032 nm, and the wavelengths of the corresponding signal and idler photons are 1290 and 860 nm, respectively. With this arrangement, according to the Raman spectra in Ref. [21], the gain of SFWM achieves the highest and the wavelength of the signal photons lies in the valley between the two adjacent peaks of fourth-order and fifth-order RS, so the background noise originating from RS is minimized.

The pump source in Fig. 1 is a mode-locked Yb-doped fiber laser with a repetition rate of 62.56 MHz. The central wavelength and full width at half-maximum (FWHM) of its output spectrum are 1042 and 25 nm, respectively. We disperse the output of the laser with a grating G. By adjusting the grating, the central wavelength and FWHM of the pump sent into the MNF are tuned to 1032 and 1.5 nm.

To separate the signal and idler photons generated in the MNF, a dichroic mirror (DM) with a cutoff length of 1250 nm is placed at the output port of the MNF. At the DM, the idler photons are reflected, while the signal photons are transmitted. In order to provide sufficient isolation from the residual pump and restrict the bandwidths of the photon pairs, two filters, F_i and F_s, are, respectively, placed in the idler and signal channels. F_i with central wavelength and FWHM of 860 and 9 nm is realized by cascading three bandpass filters (BPFs), and F_s consists of two long-pass filters with a cutoff wavelength of 1250 nm. The 18 channel coarse wavelength division multiplexer (CWDM) is used to select the wavelength of the heralded signal photons. The central wavelengths of the CWDM channels range from 1270 to 1610 nm, and the spacing between adjacent channels is 20 nm. The transmission profile of each CWDM channel is super-Gaussian shaped with a 0.5 dB bandwidth of about 18 nm. In our source, we employ the 1290 nm channel to filter the signal photons. The total transmission efficiencies for idler and signal photons are 41.8% and 38.5%, respectively.

We use the detection events of the idler photons as the heralding trigger to herald the existence of single photons. The idler photons are detected by single photon detector (SPD) SPD1 (SPCM-AQRH-15, Perkin-Elmer), which is based on a Si-avalanche photodiode (Si-APD) and has a quantum efficiency of about 50% at 860 nm. The dark counts of SPD1 are 0.1 kHz, and the dead time is set to be 40 ns. Since single mode propagation is not guaranteed for the idler photons, SPD1 is multimode-fiber pigtailed. However, based on our observation, the amount of idler photons in higher-order spatial modes is insignificant. As shown in Fig. 1, our source has two output ports: the electrical port for the heralding trigger and the optical fiber port for the heralded single photons.

The characterization system consists of a 50/50 beam splitter (BS), two InGaAs/InP-APD-based SPDs, and a computer-controlled photon counting system. The heralded signal photons from the source are sent into the BS, and the two outputs of the BS are connected to SPD2 and SPD3, respectively. SPD2 and SPD3 (ROI Optoelectronic Technology) are working in the gated Geiger mode, which are triggered by the heralding trigger. The dark counts probability per gate and gate window of both SPDs are 9.7×10^{-6} and 5 ns, respectively. Since the photon count rates are relatively low, there is no dead time applied. The quantum efficiency of SPD2 (SPD3) is ~12.0% (~11.4%) at 1290 nm.

In the experiment, we first measure the quantum correlation and background noise of the photon pairs in heralding and heralded channels. We record the individual counting rates of SPD1 and SPD2, N_t and N_s,

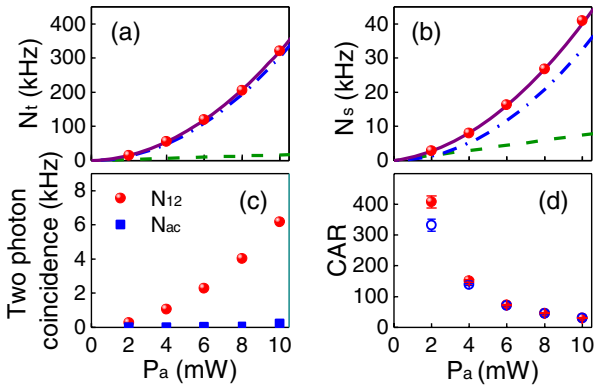

Fig. 2. (a), (b) Measured single channel counting rates in the heralding and heralded channels N_t and N_s, as a function of average pump power P_a. The solid curves in (a) and (b) are the fitting polynomial with the dashed and dot-dashed lines, respectively, representing the linear and quadratic terms. (c) Two-fold coincidence and accidental coincidence counting rates N_{12} and N_{ac}. (d) Coincidence-to-accidental ratio (CAR) as a function of P_a. The solid and hollow symbols denote results with and without subtracting the dark counts of SPDs. In (a), (b), and (c), the dark counts of SPDs are subtracted.

and the two-fold coincidence of SPD1 and SPD2 for signal and idler photons originating from the same and adjacent pulses when the pump power launched into the MNF is varied. Figures 2(a) and 2(b) show N_t and N_s as a function of pump power P_a, respectively. We fit the single counting rate N_t by using the polynomial $N_{t(s)} = \alpha_{t(s)} P_a + \beta_{t(s)} P_a^2$ and obtain the best fitting parameters $\alpha_{t(s)} = 1.66(0.75)$ kHz/mW, and $\beta_{t(s)} = 3.03(0.32)$ kHz/mW^2. The linear and quadratic terms, respectively, denote the intensity of photons that originated from RS and SFWM[22]. The results indicate that noise photons originating from RS exist in both heralding and heralded channels, but the contribution of RS is insignificant. In particular, photons from SFWM absolutely dominate in the heralding channel.

Figure 2(c) shows the coincidence rate N_{12} and accidental coincidence rate N_{ac} between SPD1 and SPD2 as a function of pump power P_a. The accidental coincidence rate is obtained by measuring the coincidence counts of signal and idler photons that are produced by different pump pulses. The coincidence-to-accidental ratio (CAR), which is calculated via $\mathrm{CAR} = N_{12}/N_{ac}$, is plotted in Fig. 2(d). It is clear that the CAR decreases with the increase of the pump power due to the increasing probability of multi-photon events. We notice that when the pump power is 10 mW, the measured CAR is ~30, which is higher than that obtained with the pump power of 9 mW in Ref. [21]. We believe the improvement of CAR is because the gain of RS for the heralding and heralded photons lies in the valley between the peaks of fourth-order and fifth-order RS.

Then, we characterize the heralding efficiency of our single photon source. The heralding efficiency H, which is defined as the probability of a single photon existing at a heralded channel when a trigger event is observed in the heralding channel, can be expressed as

$$H = \frac{N_c}{N_t}. \tag{1}$$

Here, N_c is the true coincidence rate between the signal and idler photons directly from the source, which is obtained by correcting the difference $N_{12} - N_{ac}$ with the transmission efficiencies of the 50/50 BS and the detection efficiency of SPD2. The calculated true coincidence rate N_c as a function of pump power P_a is plotted in Fig. 3(a). After substituting N_c and N_t into Eq. (1), we obtain the heralding efficiency of our source $H \approx 32\%$, which does not vary with pump power. Moreover, when the pump power is 10 mW, the count rate of heralded signal photons is up to 100 kHz. If we correct the result by assuming that the transmission efficiency of the signal channel inside the source is 100%, the heralding efficiency would be ~80%.

Finally, we characterize the second-order intensity correlation function $g^{(2)}(0)$ of the heralded single photons by using the setup in Fig. 1. For signal and idler photons originated from the same pump pulse, we measure the three-fold coincidence counts between the three SPDs as N_{123}, shown in Fig. 3(b), and two-fold coincidence counts between SPD1 and SPD2 (SPD3) as N_{12} (N_{13}). Then, we can obtain $g^{(2)}(0)$ by employing the following expression[14]:

$$g^{(2)}(0) = \frac{N_{123} N_t}{N_{12} N_{13}}. \tag{2}$$

The measured results of $g^{(2)}$ as a function of the pump power P_a are shown in Fig. 3(c). One sees that the measured $g^{(2)}(0)$ increases with pump power P_a due to the increased probability of the multi-photon events. When $P_a = 2$ mW, the emission rate of heralded single photons is about 4.6 kHz [see Fig. 3(c)], and the measured $g^{(2)}(0)$ is 0.017 ± 0.002, which is significantly less than the classical limit of unity. This result demonstrates the non-classical nature of our single photon source. When $P_a = 10$ mW, the rate of the heralded signal photons emerging from the source is up to 100 kHz, and the measured $g^{(2)}(0)$ is 0.15 ± 0.002, which is still significantly lower than the classical limit.

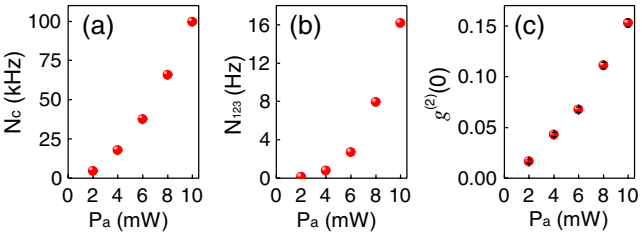

Fig. 3. (a) Measured counting rate of true coincidence N_c. (b) Measured three-fold coincidence N_{123}. (c) Measured second-order correlation function $g^{(2)}(0)$.

Because the diameter of our 15 cm long taper-drawn MNF is inhomogeneous, the FWHM of the SFWM gain spectrum is ~80 (40) nm for signal (idler) photons, which is broader than the theoretical calculated value for MNF with a uniform diameter of 0.9 μm[21]. Therefore, by taking advantage of the broader gain bandwidth, we can tune the central wavelength of our heralded signal photon source in the telecom O band within the range of 1250–1330 nm by properly managing the wavelength of heralding photons. However, if the wavelength of output single photons is tuned, the value of $g^{(2)}(0)$ for a given rate of signal photons will be increased. For example, when the central wavelength of filter F_i in the heralding channel is adjusted to 851 nm (with an FWHM of 9 nm), the heralded single photons are mainly emerging at the 1310 nm channel of the CWDM. In this case, the measured result is $g^{(2)}(0) = 0.025 \pm 0.002$ when $P_a = 2$ mW, which is slightly higher than that of the heralded single photons at 1290 nm. This is because the gain of RS at 1290 nm is the lowest in the range of 1250–1330 nm. The existence of noise photons that originated from RS in the heralded single photon sources will lead to the increase of $g^{(2)}(0)$ due to the bunching effect of RS.

In conclusion, we present a heralded single photon source at 1290 nm by using the SFWM in a taper-drawn MNF. The heralding photons at 860 nm are detected by using the commercially available Si-APD-based SPD with high quantum efficiency, which helps to increase the rate of heralded single photons. When the emission rate of the heralded signal photons is about 4.6 kHz, the measured second-order intensity correlation function $g^{(2)}(0) = 0.017 \pm 0.002$, which is suppressed by a factor of more than 55 relative to the classical limit. Moreover, by taking advantage of the broader gain bandwidth of SFWM, the central wavelength of the heralded signal photons can be tuned in the range of 1250–1330 nm by properly adjusting the wavelength of heralding photons. We believe the noise of our heralded single photon source contributed by RS can be further suppressed by using the heralding photons to control a shutter in the heralded channel[23]. Because a taper-drawn MNF is compatible with SMF fiber switches, it is convenient for improving the efficiency of the heralded single photon source by using the temporal multiplexing methods[24]. Additionally, the transmission efficiency of the taper-drawn MNF can be increased to 99% by improving the fabrication techniques[25]. Therefore, it is promising to develop the MNF-based heralded single photon source into an all-fiber device for fulfilling the task of QKD in optical fiber networks.

References

1. W. K. Wootters and W. H. Zurek, Nature **299**, 802 (1982).
2. S. M. Tan, D. F. Walls, and M. J. Collett, Phys. Rev. Lett. **66**, 252 (1991).
3. N. Gisin, G. G. Ribordy, W. Tittel, and H. Zbinden, Rev. Mod. Phys. **74**, 145 (2002).
4. P. Kok, W. J. Munro, K. Nemoto, T. C. Ralph, J. P. Dowling, and G. J. Milburn, Rev. Mod. Phys. **79**, 135 (2007).
5. P. Kumar, P. Kwiat, A. Migdall, S. W. Nam, J. Vuckovic, and F. N. C. Wong, Quantum Inf. Process. **3**, 215 (2004).
6. R. Zhao and R. Liang, Chin. Opt. Lett. **14**, 062701 (2016).
7. C. K. Hong and L. Mandel, Phys. Rev. Lett. **56**, 58 (1986).
8. F. Sylvain, A. Olivier, T. Sébastien, B. Pascal, B. Alexios, G. Nicolas, and Z. Hugo, New J. Phys. **6**, 163 (2004).
9. Z. H. Levine, J. Fan, J. Chen, A. Ling, and A. Migdall, Opt. Express **18**, 3708 (2010).
10. P. J. Mosley, J. S. Lundeen, B. J. Smith, and I. A. Walmsley, New J. Phys. **10**, 093011 (2008).
11. M. Hu, Y. Chen, G. Li, and X. Chen, Chin. Opt. Lett. **14**, 061301 (2016).
12. E. A. Goldschmidt, M. D. Eisaman, J. Fan, S. V. Polyakov, and A. Migdall, Phys. Rev. A **78**, 013844 (2008).
13. Y.-P. Huang, J. B. Altepeter, and P. Kumar, Phys. Rev. A **82**, 043826 (2010).
14. L. Yang, X. Ma, X. Guo, L. Cui, and X. Li, Phys. Rev. A **83**, 053843 (2011).
15. A. R. McMillan, J. Fulconis, M. Halder, C. Xiong, J. G. Rarity, and W. J. Wadsworth, Opt. Express **17**, 6156 (2009).
16. L. Cui, C. Guo, and X. Li, J. Mod. Opt. **60**, 1593 (2013).
17. M. Halder, J. Fulconis, B. Cemlyn, A. Clark, C. Xiong, W. J. Wadsworth, and J. G. Rarity, Opt. Express **17**, 4670 (2009).
18. L. Zhang, C. Söller, O. Cohen, B. J. Smith, and I. A. Walmsley, J. Mod. Opt. **59**, 1525 (2012).
19. R. J. A. Francis-Jones, R. A. Hoggarth, and P. J. Mosley, Optica **3**, 1270 (2016).
20. T. Zhu, F. Xiao, L. Xu, M. Liu, M. Deng, and K. S. Chiang, Opt. Express **20**, 24465 (2012).
21. L. Cui, X. Li, C. Guo, Y. H. Li, Z. Y. Xu, L. J. Wang, and W. Fang, Opt. Lett. **38**, 5063 (2013).
22. X. Li, P. Voss, J. Chen, K. Lee, and P. Kumar, Opt. Express **13**, 2236 (2005).
23. J. A. F.-J. Robert and J. M. Peter, J. Opt. **19**, 104005 (2017).
24. X. Zhang, Y. H. Lee, B. A. Bell, P. H. W. Leong, T. Rudolph, B. J. Eggleton, and C. Xiong, Opt. Express **25**, 26067 (2017).
25. J. E. Hoffman, S. Ravets, J. A. Grover, P. Solano, P. R. Kordell, J. D. Wong-Campos, L. A. Orozco, and S. L. Rolston, AIP Adv. **4**, 067124 (2014).